INTERNATIONAL JOURNAL FOR NUMERICAL METHODS IN FLUIDS, VOL. 9, 811–832 (1989)

INTERNAL WAVE REFLECTIONS AND TRANSMISSIONS ARISING FROM A NON-UNIFORM MESH. PART II: A GENERALIZED ANALYSIS FOR THE CRANK–NICOLSON LINEAR FINITE ELEMENT SCHEME

B. CATHERS
NSW Public Works Department, Hydraulics Laboratory, 110B King Street, Manly Vale, NSW, Australia, 2093

S. BATES
British Gas Corporation, Engineering Research Station, Harvey Combe, Killingworth, PO Box 1LH, Newcastle upon Tyne NE99 1LH, U.K.

R. PENOYRE
Civil Engineering Department, Simon Engineering Laboratories, Manchester University, Brunswick Street, Manchester M13 9PL, U.K.

AND

B. A. O'CONNOR
Civil Engineering Department, Liverpool University, Brownlow Street, PO Box 147, Liverpool L69 3BX, U.K.

SUMMARY

Internal wave reflections and transmissions are examined for the Crank–Nicolson linear finite element scheme applied to the linear shallow water equations in a 1D domain containing an abrupt change in nodal spacing. In Part I of this series the reflection/transmission analysis was verified by some 'hot-start' numerical experiments. Here in Part II, however, that analysis is found wanting when it comes to providing a description of the pseudo-steady state wave configuration which develops with some 'cold-start' experiments. It is shown that the analysis of Part I can be extended to take in both the 'hot-' and 'cold-start' experimental results such that four essentially different wave configurations can be identified. The four configurations are discernible on the basis of group velocity. In order to be sustained, two of the configurations require one energy source whereas the other two require two energy sources. Numerical experiments confirmed the analysis.

KEY WORDS Fourier analysis Non-uniform mesh Wave reflection/transmission Group velocity Crank–Nicolson finite elements

1. INTRODUCTION

In Part I of this series of three papers, an analysis was made of the reflected and transmitted waves arising from an incident wave impinging on an abrupt change in nodal spacing. The numerical scheme used was the Crank–Nicolson linear finite element scheme applied to the linear shallow

0271–2091/89/070811–22$11.00

Received May 1988
Revised September 1988

water equations:

$$\frac{\partial u}{\partial t}+g\frac{\partial \eta}{\partial x}=0, \tag{1}$$

$$\frac{\partial \eta}{\partial t}+h\frac{\partial u}{\partial x}=0. \tag{2}$$

The domain consisted of two contiguous regions which had a constant but different nodal spacing. Thus the only distinguishing feature between the two regions is computational rather than physical. The results of the analysis were surprising: it was shown that the products of the incident wave were two transmitted waves but *no* reflected waves, since the reflection coefficients β_1 and β_2 were both zero. If the incident wave in the upstream region (i.e. region 1) had a dimensionless wave number $\gamma_{1a}=\sigma_{1a}\Delta x_1$, then the two transmitted waves in the downstream region (i.e. region 2) had wave numbers $\gamma_{2a}=\sigma_{2a}\Delta x_2$ and $\gamma_{2b}=\sigma_{2b}\Delta x_2$ which are related by

$$\tan(\gamma_{2a}/2)\tan(\gamma_{2b}/2)=3. \tag{3}$$

These results of the analysis were confirmed by 'hot-start' numerical experiments. In the 'hot-start' experiments, the initial conditions consisted of filling the upstream region with the incident wave and the downstream region with the two transmitted waves together with the appropriate amplitudes and phases. The somewhat unusual feature of the Crank–Nicolson FE scheme, compared, for example, with wave equation schemes, is that the dispersion relation is hill-shaped or 'concave down' rather than monotonically increasing.

In this paper several 'cold-start' experiments were carried out and it is shown that for them the analysis of Part I is not the whole story. By generalizing the analysis, however, four possible wave configurations can be identified; of these, two correspond to the 'hot-start' experiments in Part I[1] and another corresponds to the 'cold-start' experiments in the present paper.

2. 'COLD-START' NUMERICAL EXPERIMENTS

The term 'cold-start' is used here to describe the initial conditions throughout the downstream region in which the dependent variables (u and η) were set to zero. The upstream region was filled with incident waves as far as the interfacial node. The upstream boundary condition was unchanged from the 'hot-start' tests in which the surface elevation at the upstream end varied sinusoidally with time.

In the computer runs, the desired initial conditions of having only an incident wave in region 1 were effected by setting both the transmission coefficients (τ_1 and τ_2) equal to zero. (These values were recorded in each window at the base of the plots.) In the *hot-start* tests of Part I (and also later in the present paper), the correctness of the analytical solution in predicting the actual numerical results was highlighted by plotting their differences (i.e. between the predicted and actual values) with small triangles at each node location. Thus a zero value at each and every node indicates a valid analysis. In the context of a *cold-start* experiment, however, with τ_1 and τ_2 set to zero in the analytical expressions (see equations (43) and (44) of Part I), this is obviously no longer the case. Nevertheless, the small triangles were found to be of great assistance in identifying the presence of waves other than the incident and transmitted waves.

The cold-start experiments were not carried out for $2\Delta x$ waves, since for this wavelength the numerical group velocity ($C_{g\mathrm{num}}=-3\sqrt{(gh)}$) is negative irrespective of the Courant number. In a 'cold-start' experiment this would result in the incident wave moving off in the upstream direction without penetrating the downstream region.

Table I. Data for the 'cold-start' numerical experiments on wave reflection and transmission; $H' = \Delta x_2/\Delta x_1$ is the mesh size ratio and N_x is the dimensionless wavelength

	Mesh expansion, $H' = 2$	Mesh contraction, $H' = 1/2$
$N_x = 4$	$L_{2a}/\Delta x_2 = 4{\cdot}0000$ $L_{1a}/\Delta x_1 = 8{\cdot}3617$ $\tau_1 = \tau_2 = 0$ $\beta_1 = \beta_2 = 0$ (Figure 1(a))	$L_{1a}/\Delta x_1 = 4{\cdot}0000$ $L_{2a}/\Delta x_2 = 8{\cdot}3617$ $\tau_1 = \tau_2 = 0$ $\beta_1 = \beta_2 = 0$ (Figure 3(a))
$N_x = 8$	$L_{2a}/\Delta x_2 = 8{\cdot}0000$ $L_{1a}/\Delta x_1 = 16{\cdot}0343$ $\tau_1 = \tau_2 = 0$ $\beta_1 = \beta_2 = 0$ (Figure 2(a))	$L_{1a}/\Delta x_1 = 8{\cdot}0000$ $L_{2a}/\Delta x_2 = 16{\cdot}0343$ $\tau_1 = \tau_2 = 0$ $\beta_1 = \beta_2 = 0$ (Figure 4(a))

2.1. Data used in the 'cold-start' numerical experiments

The data used in the four tests are given in Table I.

2.2. Results and conclusions of the 'cold-start' numerical experiments

The graphical output from the 'cold-start' numerical tests is contained in Figures 1(a)–4(a). The two most notable features of this series of experiments were:

(i) In the downstream region, there appeared to be only a single transmitted wave present. Moreover, its wavelength pertained to the physical wave number rather than the complementary non-physical wave number.

(ii) In the upstream region, the incident wave had a high-wave-number component superimposed on it. This high-wave-number disturbance emanated from the interface and had a wavelength between $2\Delta x_1$ and $3\Delta x_1$. Its wavelength and amplitude were the same as the waveform of the residuals and are easily seen in region 1 of the figures.

Since the disturbance had wavelengths less than $3\Delta x_1$, it was associated with a negative group velocity but a positive phase velocity. The implication here therefore is that the picture which was developing in region 1 of each of these cold-start experiments was of two incident waves impinging on the interface! This gave rise to a single 'physical' transmitted wave in region 2. Hence the pattern of waves which developed in the 'cold-start' experiments consisted of two incident waves (apparently with complementary wave numbers) in region 1 and a single transmitted wave in region 2. Clearly the 'hot-start' analysis of Part I, which does provide a valid solution to the finite element equations, does not provide a correct description for the 'cold-start' experiments. It appears that there are at least two different configurations of waves. In order to explain these results, the analysis for the 'hot-start' experiments was re-examined.

3. GENERALIZED ANALYSIS TO INCLUDE THE 'COLD-START' NUMERICAL EXPERIMENTS

It was noted that the 'cold-start' experiments were characterized by two incident waves with complementary wave numbers. Such a wave pattern could be achieved by superimposing two 'hot-start' solutions in which the two incident wave numbers are complementary. Figure 5(a)

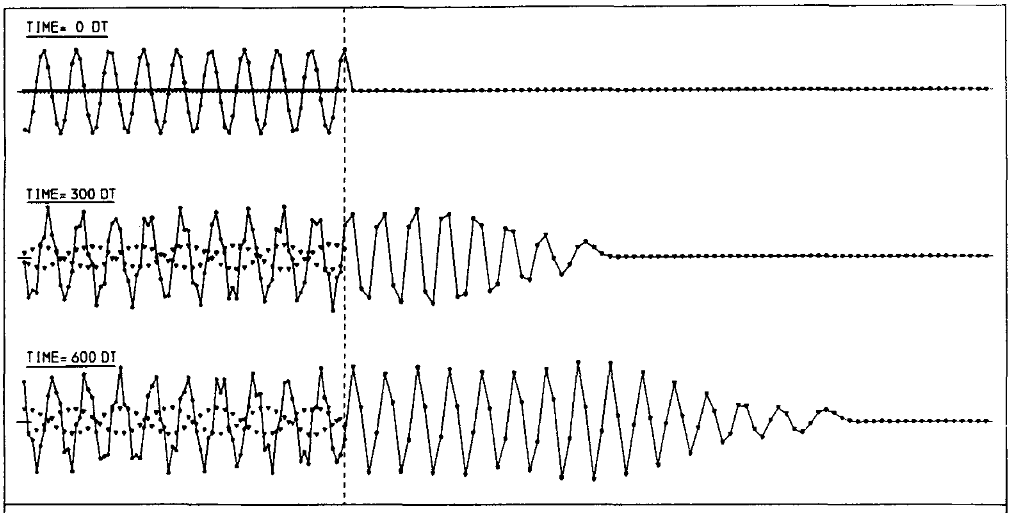

TEST CONDITIONS : DT= 0.2 (S) , CELERITY= 1.00 (M/S) , MEAN DEPTH=1/9.81 (M) CONSISTENT MASS LINEAR ELEMENTS

▽ DENOTES THE RESIDUAL = NUMERICAL SOLUTION FROM MODEL - NUMERICAL PREDICTION FROM ANALYSIS
LHS REGION : DX= 1.0 (M) , COURANT NO.= 0.20, L/DX= 8.3617, REFLECTION COEFFICIENT= (0.00000E00 , 0.00000E00)
RHS REGION : DX= 2.0 (M) , COURANT NO.= 0.10, L/DX= 4.0000, TRANSMISSION COEFFICIENT= (0.00000E00 , 0.00000E00)
L/DX= 2.5152, TRANSMISSION COEFFICIENT= (0.00000E00 , 0.00000E00)

EXPERIMENTS FOR WAVE REFLECTIONS DUE TO A CHANGE IN MESH SIZE FOR THE SHALLOW WATER EQUATIONS

Figure 1(a). Mesh expansion test with cold start. At $t=0$, the only wave present is the incident wave ($8\cdot3617\Delta x_1$)

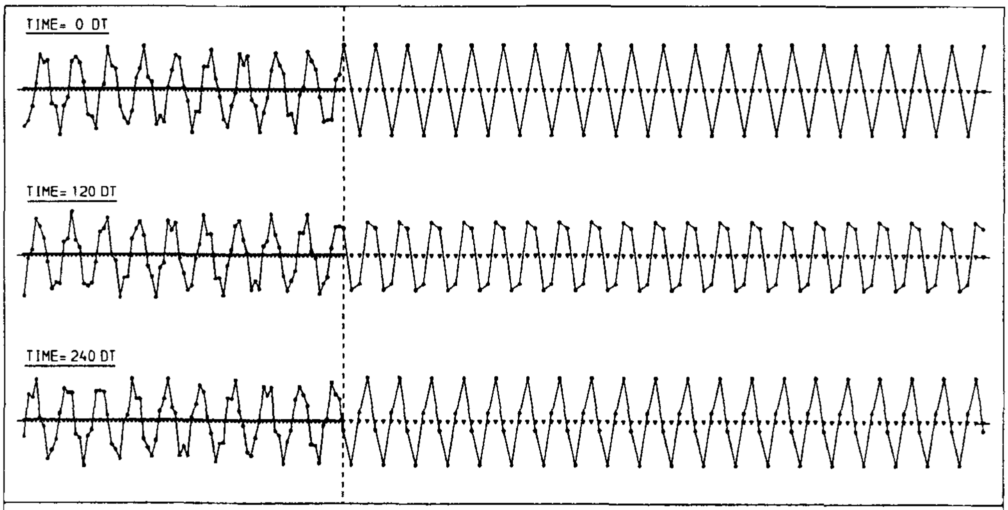

TEST CONDITIONS : DT= 0.2 (S) , CELERITY= 1.00 (M/S) , MEAN DEPTH=1/9.81 (M) CONSISTENT MASS LINEAR ELEMENTS

▽ DENOTES THE RESIDUAL = NUMERICAL SOLUTION FROM MODEL - NUMERICAL PREDICTION FROM ANALYSIS
LHS REGION : DX= 1.0 (M) , COURANT NO.= 0.20, L/DX= 8.3617, RELATIVE WAVE AMPLITUDE, A= 0.10000E01
L/DX= 2.1816, RELATIVE WAVE AMPLITUDE, B= 0.28642E00
RHS REGION : DX= 2.0 (M) , COURANT NO.= 0.10, L/DX= 4.0000, RELATIVE WAVE AMPLITUDE, C= 0.12864E01
L/DX= 2.5152, RELATIVE WAVE AMPLITUDE, D= 0.00000E00

EXPERIMENTS FOR WAVE REFLECTIONS DUE TO A CHANGE IN MESH SIZE FOR THE SHALLOW WATER EQUATIONS

Figure 1(b). Mesh expansion test with hot start for case (ii) with $D=0$. Waves present are: incident waves A ($8\cdot3617\Delta x_1$) and B ($2\cdot1816\Delta x_1$), and transmitted wave C ($4\cdot0000\Delta x_2$)

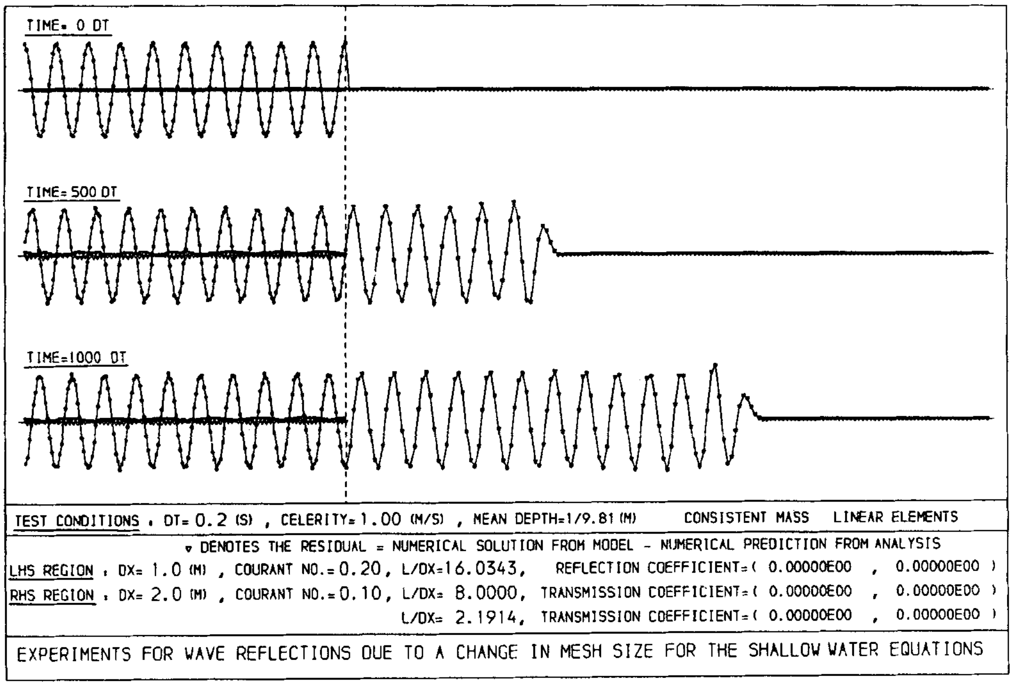

```
TEST CONDITIONS , DT= 0.2 (S) , CELERITY= 1.00 (M/S) , MEAN DEPTH=1/9.81 (M)      CONSISTENT MASS   LINEAR ELEMENTS
                    ▿ DENOTES THE RESIDUAL = NUMERICAL SOLUTION FROM MODEL - NUMERICAL PREDICTION FROM ANALYSIS
LHS REGION , DX= 1.0 (M) , COURANT NO.=0.20, L/DX=16.0343,   REFLECTION COEFFICIENT=( 0.00000E00   ,  0.00000E00 )
RHS REGION , DX= 2.0 (M) , COURANT NO.=0.10, L/DX= 8.0000, TRANSMISSION COEFFICIENT=( 0.00000E00   ,  0.00000E00 )
                                             L/DX= 2.1914, TRANSMISSION COEFFICIENT=( 0.00000E00   ,  0.00000E00 )
EXPERIMENTS FOR WAVE REFLECTIONS DUE TO A CHANGE IN MESH SIZE FOR THE SHALLOW WATER EQUATIONS
```

Figure 2(a). Mesh expansion test with cold start. At $t=0$, the only wave present is the incident wave ($16{\cdot}0343\Delta x_1$)

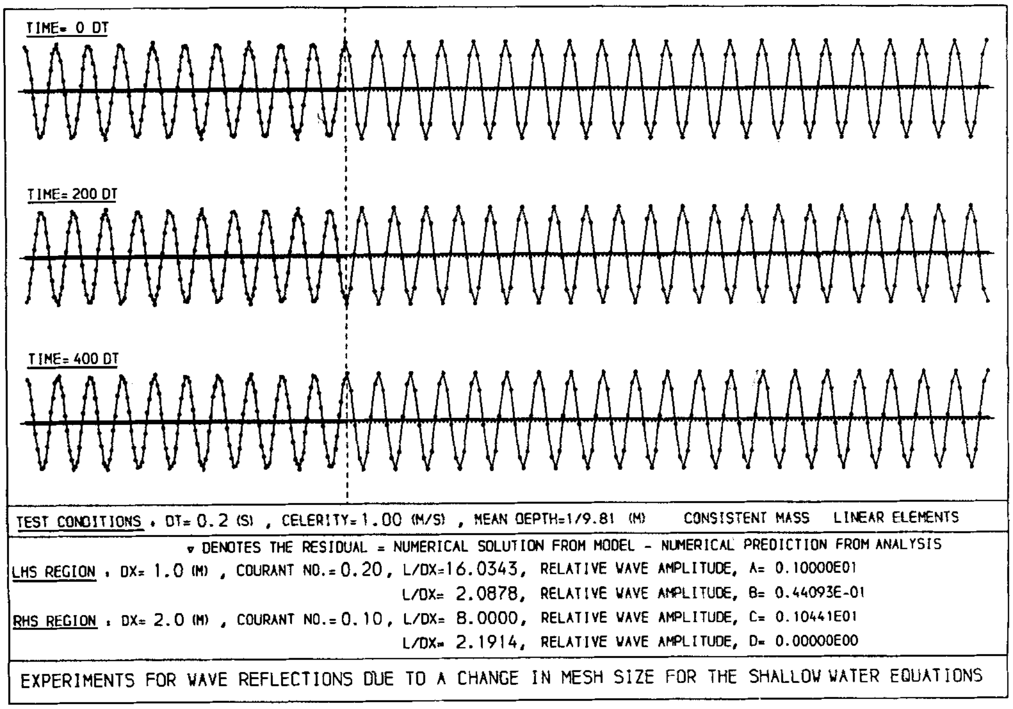

```
TEST CONDITIONS , DT= 0.2 (S) , CELERITY= 1.00 (M/S) , MEAN DEPTH=1/9.81 (M)      CONSISTENT MASS   LINEAR ELEMENTS
                    ▿ DENOTES THE RESIDUAL = NUMERICAL SOLUTION FROM MODEL - NUMERICAL PREDICTION FROM ANALYSIS
LHS REGION , DX= 1.0 (M) , COURANT NO.=0.20, L/DX=16.0343, RELATIVE WAVE AMPLITUDE, A= 0.10000E01
                                             L/DX= 2.0878, RELATIVE WAVE AMPLITUDE, B= 0.44093E-01
RHS REGION , DX= 2.0 (M) , COURANT NO.=0.10, L/DX= 8.0000, RELATIVE WAVE AMPLITUDE, C= 0.10441E01
                                             L/DX= 2.1914, RELATIVE WAVE AMPLITUDE, D= 0.00000E00
EXPERIMENTS FOR WAVE REFLECTIONS DUE TO A CHANGE IN MESH SIZE FOR THE SHALLOW WATER EQUATIONS
```

Figure 2(b). Mesh expansion test with hot start for case (ii) with $D=0$. Waves present are: incident waves A ($16{\cdot}0343\Delta x_1$) and B ($2{\cdot}0878\Delta x_1$), and transmitted wave C ($8{\cdot}0000\Delta x_2$)

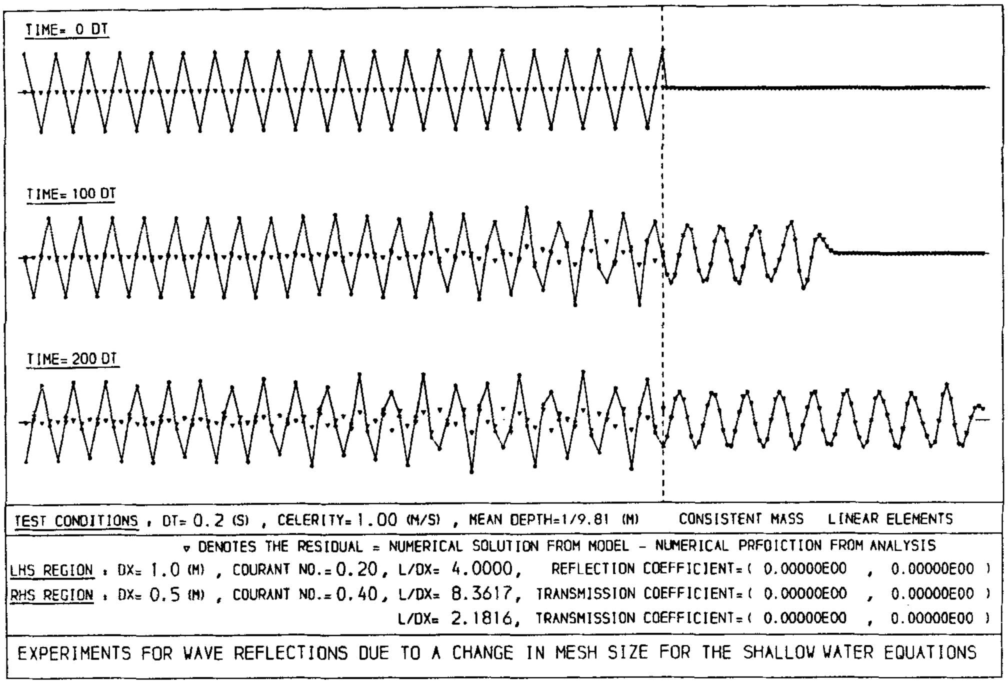

```
TEST CONDITIONS , DT= 0.2 (S) , CELERITY= 1.00 (M/S) , MEAN DEPTH=1/9.81 (M)     CONSISTENT MASS   LINEAR ELEMENTS
                  ▿ DENOTES THE RESIDUAL = NUMERICAL SOLUTION FROM MODEL - NUMERICAL PRFOICTION FROM ANALYSIS
LHS REGION : DX= 1.0 (M) , COURANT NO.=0.20, L/DX= 4.0000,   REFLECTION COEFFICIENT=( 0.00000E00  ,  0.00000E00 )
RHS REGION : DX= 0.5 (M) , COURANT NO.=0.40, L/DX= 8.3617, TRANSMISSION COEFFICIENT=( 0.00000E00  ,  0.00000E00 )
                                             L/DX= 2.1816, TRANSMISSION COEFFICIENT=( 0.00000E00  ,  0.00000E00 )
EXPERIMENTS FOR WAVE REFLECTIONS DUE TO A CHANGE IN MESH SIZE FOR THE SHALLOW WATER EQUATIONS
```

Figure 3(a). Mesh refinement test with cold start. At $t=0$, the only wave present is the incident wave ($4{\cdot}0000\Delta x_1$)

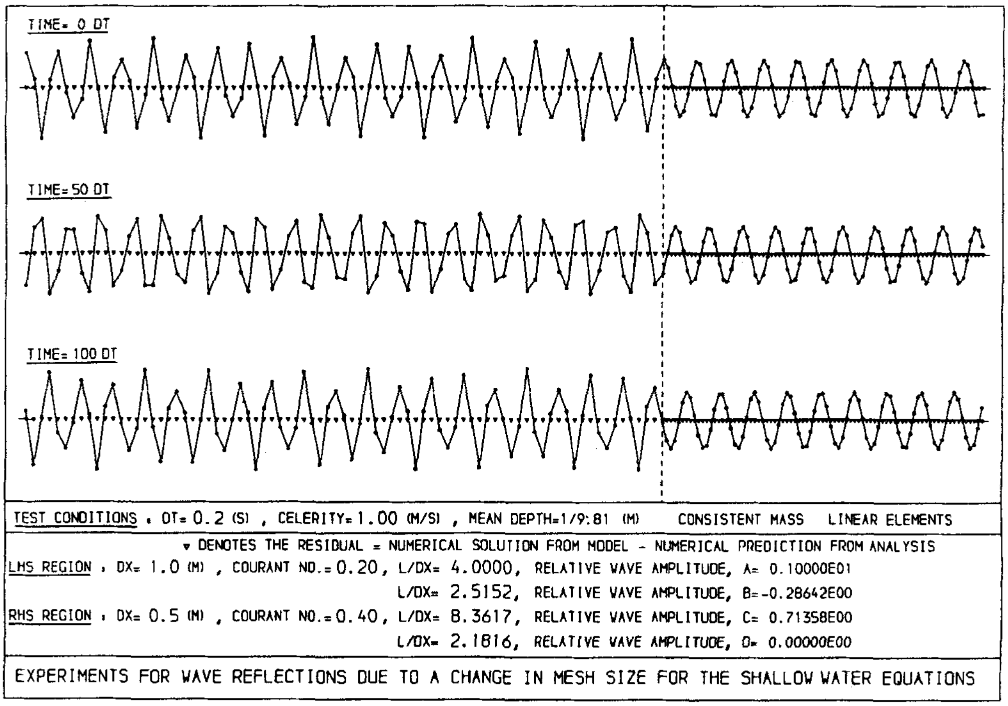

```
TEST CONDITIONS , DT= 0.2 (S) , CELERITY= 1.00 (M/S) , MEAN DEPTH=1/9:81 (M)     CONSISTENT MASS   LINEAR ELEMENTS
                  ▿ DENOTES THE RESIDUAL = NUMERICAL SOLUTION FROM MODEL - NUMERICAL PREDICTION FROM ANALYSIS
LHS REGION , DX= 1.0 (M) , COURANT NO.=0.20, L/DX= 4.0000, RELATIVE WAVE AMPLITUDE, A= 0.10000E01
                                             L/DX= 2.5152, RELATIVE WAVE AMPLITUDE, B=-0.28642E00
RHS REGION , DX= 0.5 (M) , COURANT NO.=0.40, L/DX= 8.3617, RELATIVE WAVE AMPLITUDE, C= 0.71358E00
                                             L/DX= 2.1816, RELATIVE WAVE AMPLITUDE, D= 0.00000E00
EXPERIMENTS FOR WAVE REFLECTIONS DUE TO A CHANGE IN MESH SIZE FOR THE SHALLOW WATER EQUATIONS
```

Figure 3(b). Mesh refinement test with hot start for case (ii) with $D=0$. Waves present are: incident waves A ($4{\cdot}0000\Delta x_1$) and B ($2{\cdot}5152\Delta x_1$), and transmitted wave C ($8{\cdot}3617\Delta x_2$)

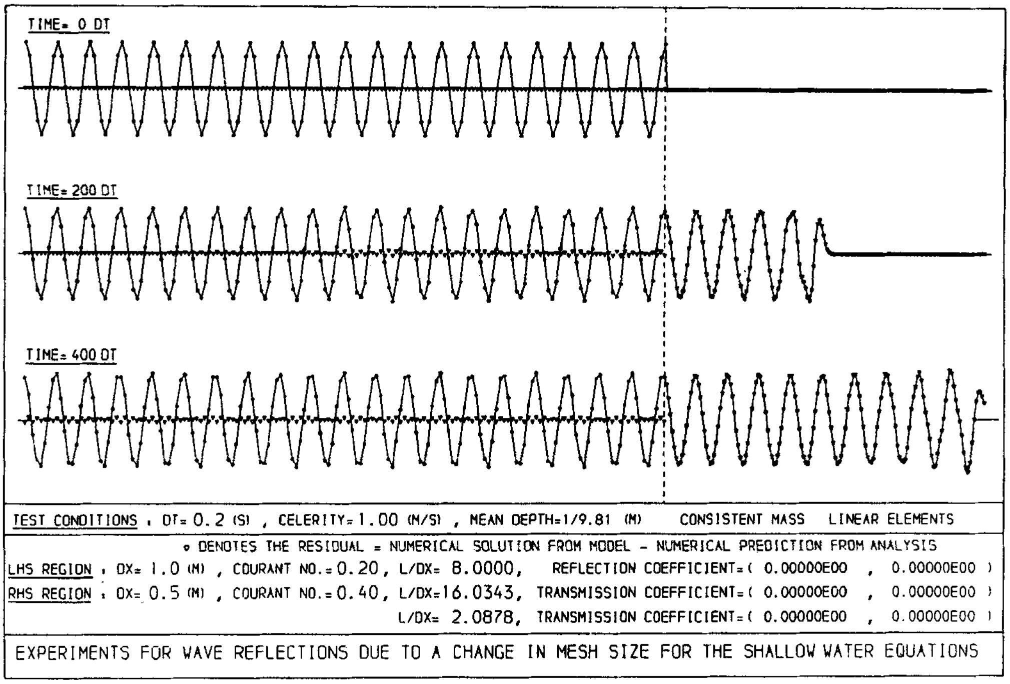

```
TEST CONDITIONS , DT= 0.2 (S) , CELERITY= 1.00 (M/S) , MEAN DEPTH=1/9.81 (M)    CONSISTENT MASS   LINEAR ELEMENTS
                  ▿ DENOTES THE RESIDUAL = NUMERICAL SOLUTION FROM MODEL - NUMERICAL PREDICTION FROM ANALYSIS
LHS REGION , DX= 1.0 (M) , COURANT NO.=0.20, L/DX= 8.0000,  REFLECTION COEFFICIENT=( 0.00000E00  , 0.00000E00 )
RHS REGION , DX= 0.5 (M) , COURANT NO.=0.40, L/DX=16.0343, TRANSMISSION COEFFICIENT=( 0.00000E00  , 0.00000E00 )
                                             L/DX= 2.0878, TRANSMISSION COEFFICIENT=( 0.00000E00  , 0.00000E00 )
EXPERIMENTS FOR WAVE REFLECTIONS DUE TO A CHANGE IN MESH SIZE FOR THE SHALLOW WATER EQUATIONS
```

Figure 4(a). Mesh refinement test with cold start. At $t=0$, the only wave present is the incident wave ($8{\cdot}0000\Delta x_1$)

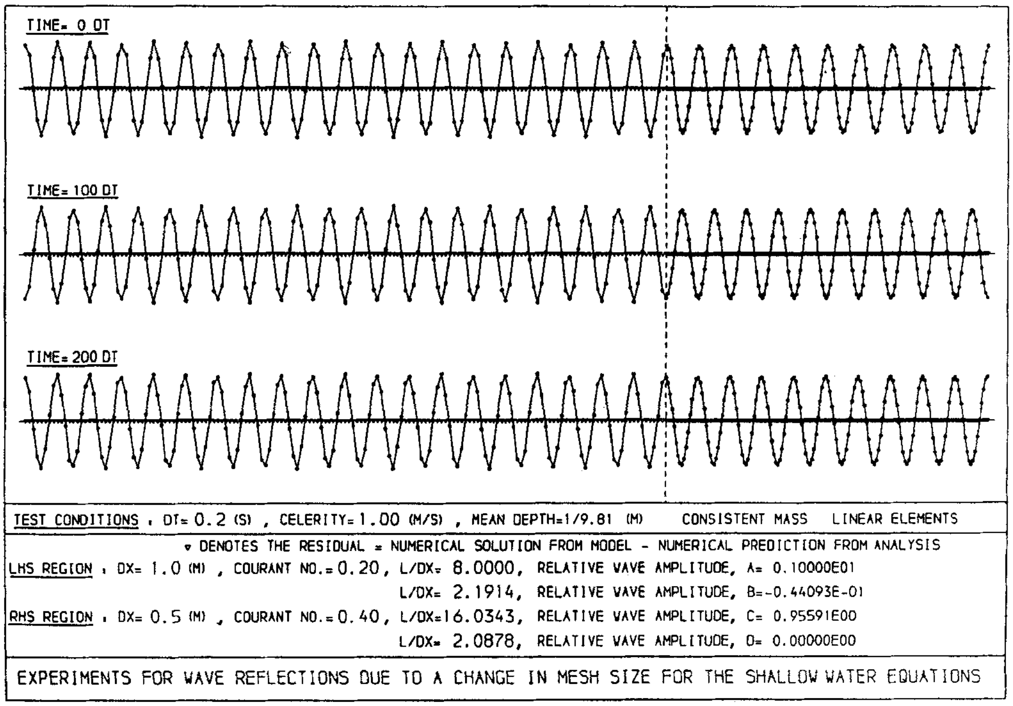

```
TEST CONDITIONS , DT= 0.2 (S) , CELERITY= 1.00 (M/S) , MEAN DEPTH=1/9.81 (M)    CONSISTENT MASS   LINEAR ELEMENTS
                  ▿ DENOTES THE RESIDUAL = NUMERICAL SOLUTION FROM MODEL - NUMERICAL PREDICTION FROM ANALYSIS
LHS REGION , DX= 1.0 (M) , COURANT NO.=0.20, L/DX= 8.0000, RELATIVE WAVE AMPLITUDE, A= 0.10000E01
                                             L/DX= 2.1914, RELATIVE WAVE AMPLITUDE, B=-0.44093E-01
RHS REGION , DX= 0.5 (M) , COURANT NO.=0.40, L/DX=16.0343, RELATIVE WAVE AMPLITUDE, C= 0.95591E00
                                             L/DX= 2.0878, RELATIVE WAVE AMPLITUDE, D= 0.00000E00
EXPERIMENTS FOR WAVE REFLECTIONS DUE TO A CHANGE IN MESH SIZE FOR THE SHALLOW WATER EQUATIONS
```

Figure 4(b). Mesh refinement test with hot start for case (ii) with $D=0$. Waves present are: incident waves A ($8{\cdot}0000\Delta x_1$) and B ($2{\cdot}1914\Delta x_1$), and transmitted wave C ($16{\cdot}0343\Delta x_2$)

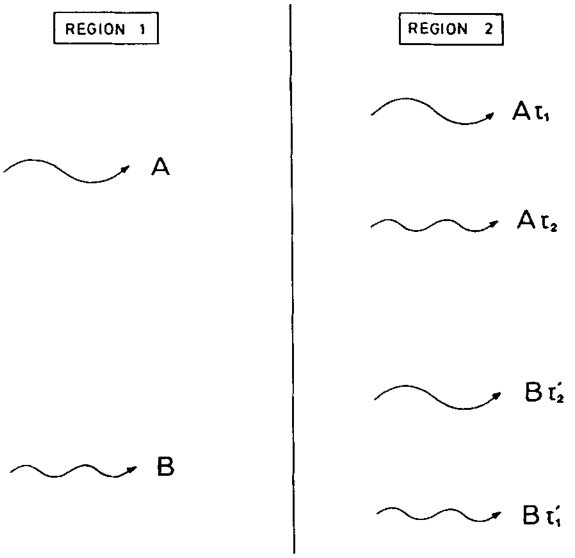

Figure 5(a). Two wave systems combined

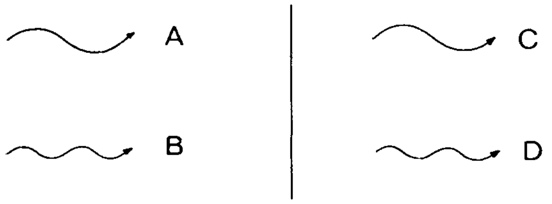

Figure 5(b). Equivalent wave system

details the combination of two incident waves and their associated transmitted waves. The convention (from Part I) of labelling the wave numbers according to the region and whether or not it is the physical wave or its complement (i.e. σ_{1_a}, σ_{1_b}, σ_{2_a}, σ_{2_b}) which is being referred to will be modified. The new convention adopted for wave numbers refers to the region and whether the wavelength is long (taken to mean greater than $3\Delta x$) or short (i.e. less than $3\Delta x$). These wave numbers are referred to as σ_A, σ_B, σ_C, σ_D.

Referring to Figure 5(a), the first incident wave has (complex) amplitude A and wave number σ_A. This wave refers specifically to the *long* wave (i.e. wavelength greater than $3\Delta x_1$) in region 1. In region 2 it gives rise to the 'physical' transmitted wave with amplitude $A\tau_1$ and low wave number σ_C, as well as the complementary transmitted wave with amplitude $A\tau_2$ and high wave number σ_D (i.e. wavelength less than $3\Delta x_1$). Equations (39) and (40) of Part I (or equations (6) and (7) below) define τ_1 and τ_2.

The second incident wave has (complex) amplitude B and wave number σ_B. This wave refers specifically to the *short* wave (i.e. wavelength less than $3\Delta x_1$) in region 1. In region 2 it gives rise to the 'physical' transmitted wave with amplitude $B\tau_1'$ and high wave number σ_D, as well as the complementary transmitted wave with amplitude $B\tau_2'$ and low wave number σ_C.

The addition of the two wave systems (Figure 5(b)) due to the two incident waves (A and B) gives rise to two transmitted waves C and D. By superposition,

$$C=A\tau_1+B\tau_2', \tag{4}$$

$$D=B\tau_1'+A\tau_2, \tag{5}$$

where from equations (39) and (40) in Part I we have

$$\tau_1=\frac{1}{2}\left[1+\frac{E_A}{E_C}\right], \tag{6}$$

$$\tau_2=\frac{1}{2}\left[1-\frac{E_A}{E_C}\right], \tag{7}$$

where

$$E_A=\frac{1+2\cos\gamma_A}{2+\cos\gamma_A}, \tag{8}$$

$$E_B=\frac{1+2\cos\gamma_B}{2+\cos\gamma_B}, \tag{9}$$

$$E_C=\frac{1+2\cos\gamma_C}{2+\cos\gamma_C}, \tag{10}$$

$$E_D=\frac{1+2\cos\gamma_D}{2+\cos\gamma_D}. \tag{11}$$

Similarly,

$$\tau_1'=\frac{1}{2}\left[1+\frac{E_B}{E_D}\right]=\tau_1 \quad \text{(using equations (8)–(11), (26), (27)),} \tag{12}$$

$$\tau_2'=\frac{1}{2}\left[1-\frac{E_B}{E_D}\right]=1-\tau_1'=\tau_2 \quad \text{(using equations (8)–(11), (26), (27)).} \tag{13}$$

For convenience, the various waves will simply be referred to by their amplitudes as wave A, B, C or D.

As for the 'hot-start' analysis, α will be used to denote the (complex) amplitude of the interfacial node in this combined wave system.

In region 1, where $x<0$, the combined instantaneous surface elevation and velocity are given by

$$\eta(x,t)=Ae^{i(\omega t-\sigma_A x)}+Be^{i(\omega t-\sigma_B x)}, \tag{14}$$

$$u(x,t)=\sqrt{(g/h)}\,(Ae^{i(\omega t-\sigma_A x)}+Be^{i(\omega t-\sigma_B x)}); \tag{15}$$

in region 2, where $x>0$, the surface elevation and velocity are

$$\eta(x,t)=Ce^{i(\omega t-\sigma_C x)}+De^{i(\omega t-\sigma_D x)}, \tag{16}$$

$$u(x,t)=\sqrt{(g/h)}\,(Ce^{i(\omega t-\sigma_C x)}+De^{i(\omega t-\sigma_D x)}); \tag{17}$$

and at the interfacial node, where $x=0$, the surface elevation and velocity are

$$\eta(0,t)=\alpha e^{i\omega t}, \tag{18}$$

$$u(0,t)=\sqrt{(g/h)}\alpha e^{i\omega t}. \tag{19}$$

It is noteworthy that waves A, B, C and D *all* travel in the downstream direction, i.e. in the positive x-direction. That is, waves A, B, C and D all have positive phase velocity (but only waves A and C have a positive group velocity).

Also, since σ_A and σ_B are complementary wave numbers as well as σ_C and σ_D, we know from equation (3) that

$$\tan(\gamma_A/2)\tan(\gamma_B/2)=\tan(\gamma_C/2)\tan(\gamma_D/2)=3. \tag{20}$$

The five unknowns are A, B, C, D and α, but since the solution being sought to explain the results of the 'cold-start' experiments has only three waves present, one of the amplitudes (i.e. D) will later be set to zero. The amplitudes B and C will be expressed in terms of the incident wave amplitude A. It is clear, however, that by setting one of A, B or C to zero instead of D, there are three more possible wave configurations consisting of three waves in each configuration. In the meantime, all four amplitudes will be retained to keep the analysis general. In each case only three equations are required in order to solve for α and two amplitudes out of A, B, C and D.

3.1. *Continuity of surface elevation at* $x=0$

Two equations can be obtained from the fact that the assumed solutions for the two regions as well as the interfacial node must be equal at the origin for all times in order to maintain continuity of the water surface (and hence also of pressure) between the two regions; i.e.

$$\eta_{x\leqslant 0}=\eta_{x=0}=\eta_{x\geqslant 0}$$

or, at $x=0$,

$$A\mathrm{e}^{\mathrm{i}(\omega t-\sigma_A x)}+B\mathrm{e}^{\mathrm{i}(\omega t-\sigma_B x)}=\alpha\mathrm{e}^{\mathrm{i}\omega t}=C\mathrm{e}^{\mathrm{i}(\omega t-\sigma_C x)}+D\mathrm{e}^{\mathrm{i}(\omega t-\sigma_D x)}.$$

Therefore

$$A+B=\alpha=C+D, \tag{21}$$

where C and D are related to A and B via equations (4) and (5).

3.2. *Momentum equation centred about* $x=0$

The third equation can be obtained by applying the Crank–Nicolson linear finite element discrete analogue of the momentum (or continuity) equation about the origin:

$$\frac{\Delta x_1}{6}\left[\left(\frac{u^{n+1}-u^n}{\Delta t}\right)_{-1}+2\left(\frac{u^{n+1}-u^n}{\Delta t}\right)_0\right]+\frac{\Delta x_2}{6}\left[2\left(\frac{u^{n+1}-u^n}{\Delta t}\right)_0+\left(\frac{u^{n+1}-u^n}{\Delta t}\right)_1\right]$$
$$+\frac{g}{4}(\eta_1-\eta_{-1})^{n+1}+\frac{g}{4}(\eta_1-\eta_{-1})^n=0. \tag{22}$$

Substitution of the appropriate assumed solutions (equations (14)–(19)) into the above gives

$$\frac{\Delta x_1}{6\Delta t}\left[\sqrt{\frac{g}{h}}(A\mathrm{e}^{\mathrm{i}[\omega(n+1)\Delta t+\gamma_A]}+B\mathrm{e}^{\mathrm{i}[\omega(n+1)\Delta t+\gamma_B]})-\sqrt{\frac{g}{h}}(A\mathrm{e}^{\mathrm{i}[\omega n\Delta t+\gamma_A]}+B\mathrm{e}^{\mathrm{i}[\omega n\Delta t+\gamma_B]})\right.$$
$$\left.+2\sqrt{\frac{g}{h}}\alpha\mathrm{e}^{\mathrm{i}\omega(n+1)\Delta t}-2\sqrt{\frac{g}{h}}\alpha\mathrm{e}^{\mathrm{i}\omega n\Delta t}\right]+\frac{\Delta x_2}{6\Delta t}\left[2\sqrt{\frac{g}{h}}\alpha\mathrm{e}^{\mathrm{i}\omega(n+1)\Delta t}-2\sqrt{\frac{g}{h}}\alpha\mathrm{e}^{\mathrm{i}\omega n\Delta t}\right.$$
$$\left.+\sqrt{\frac{g}{h}}(C\mathrm{e}^{\mathrm{i}[\omega(n+1)\Delta t-\gamma_C]}+D\mathrm{e}^{\mathrm{i}[\omega(n+1)\Delta t-\gamma_D]})-\sqrt{\frac{g}{h}}(C\mathrm{e}^{\mathrm{i}[\omega n\Delta t-\gamma_C]}+D\mathrm{e}^{\mathrm{i}[\omega n\Delta t-\gamma_D]})\right]$$

$$+\frac{g}{4}\left[Ce^{i[\omega(n+1)\Delta t-\gamma_C]}+De^{i[\omega(n+1)\Delta t-\gamma_D]}-(Ae^{i[\omega n\Delta t+\gamma_A]}+Be^{i[\omega n\Delta t+\gamma_B]})\right]$$

$$+\frac{g}{4}\left[Ce^{i[\omega n\Delta t-\gamma_C]}+De^{i[\omega n\Delta t-\gamma_D]}-(Ae^{i[\omega n\Delta t+\gamma_A]}+Be^{i[\omega n\Delta t+\gamma_B]})\right]=0. \tag{23}$$

From the dispersion relation for the two regions, it is easily shown that

$$\frac{\lambda-1}{\lambda+1}=i\left(\frac{1\cdot5\not{C}_1\sin\gamma_A}{2+\cos\gamma_A}\right)=i\left(\frac{1\cdot5\not{C}_1\sin\gamma_B}{2+\cos\gamma_B}\right)=i\left(\frac{1\cdot5\not{C}_2\sin\gamma_C}{2+\cos\gamma_C}\right)=i\left(\frac{1\cdot5\not{C}_2\sin\gamma_D}{2+\cos\gamma_D}\right), \tag{24}$$

and substitution of equation (21) (to eliminate α) and equation (24) into (23) leads to the simplified form of equation (23):

$$-(E_AA+E_BB)+E_CC+E_DD=0. \tag{25}$$

Using equation (20), it is easily shown that

$$E_A=-E_B, \tag{26}$$

$$E_C=-E_D. \tag{27}$$

3.3. Summary of equations to be solved

The two equations to be solved for two unknowns out of the four amplitudes A, B, C and D are

$$A+B-C-D=0, \tag{21}$$

$$-(E_AA+E_BB)+E_CC+E_DD=0, \tag{25}$$

where E_A, E_B, E_C and E_D are defined by equations (8)–(11).

3.4. Solutions of the equations

The solutions being sought to equations (21) and (25) contain three waves only. It is seen therefore that setting each of A, B, C and D to zero in turn gives four possible different solutions or wave configurations, which are represented in Figure 6 as cases (iii), (i), (iv) and (ii) respectively.

The first solution to be discussed has $B=0$ and, as a check, should coincide with the 'hot-start' solution of equations (41)–(44) of Part I.

Case (i): $B=0$. As this case corresponds to all but two of the 'hot-start' experiments carried out in Part I (i.e. Figures 12, 13, 15 and 16), it is referred to as the 'hot-start'. The unknown transmitted wave amplitudes C and D will be found relative to the incident wave amplitude A. Solving equations (21) and (25) simultaneously gives

$$\frac{C}{A}=0\cdot5\left[1+\frac{E_A}{E_C}\right]=0\cdot5\left[1+\frac{\left(\dfrac{1+2\cos\gamma_A}{2+\cos\gamma_A}\right)}{\left(\dfrac{1+2\cos\gamma_C}{2+\cos\gamma_C}\right)}\right], \tag{28}$$

$$\frac{D}{A}=0\cdot5\left[1-\frac{E_A}{E_C}\right]=0\cdot5\left[1-\frac{\left(\dfrac{1+2\cos\gamma_A}{2+\cos\gamma_A}\right)}{\left(\dfrac{1+2\cos\gamma_C}{2+\cos\gamma_C}\right)}\right], \tag{29}$$

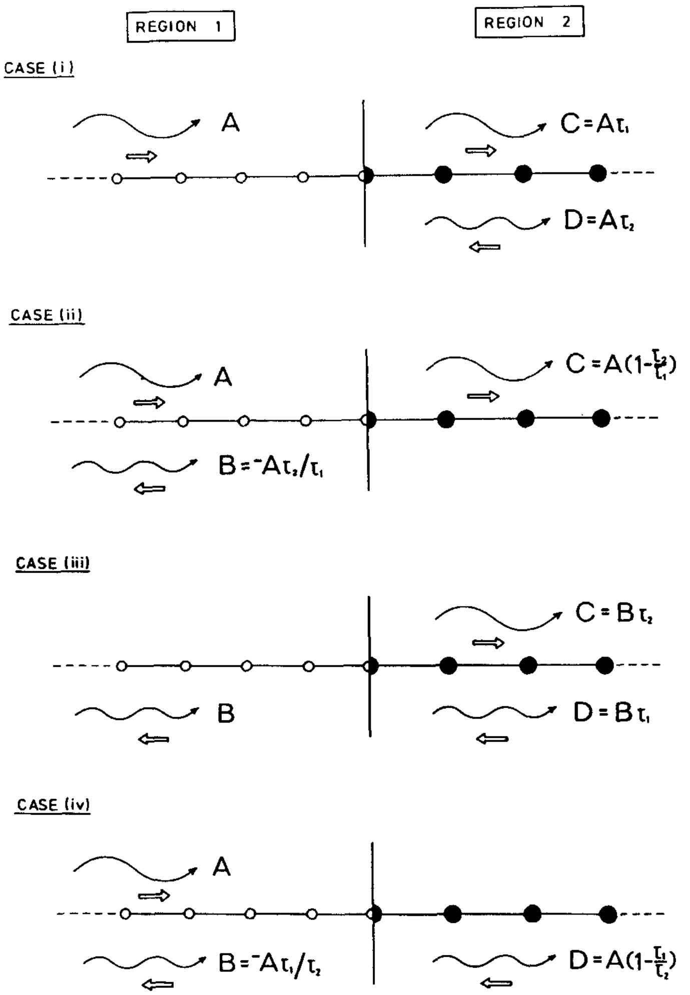

Figure 6. Schematics of the four wave configurations—directions of energy flux are indicated by an arrow (⇒)

which are identical to equations (6) and (7) for τ_1 and τ_2 respectively. Numerical experiments confirming the validity of the analysis for this case have already been discussed in Part I. The relevant figures (for equations (28) and (29)) are Figures 5–9 in Part I.[1]

Case (ii): $D=0$. This is the case which will be referred to as the 'cold-start', since it explains what happens in the model with the particular 'cold-start' described in Section 2. The unknown amplitudes B and C will be found relative to the incident wave amplitude A. The solution of equations (21) and (25) yields

$$\frac{B}{A}=\frac{E_{\mathrm{A}}-E_{\mathrm{C}}}{E_{\mathrm{A}}+E_{\mathrm{C}}}=\frac{-\tau_2}{\tau_1} \quad \text{(using equation (5)),} \tag{30}$$

$$\frac{C}{A}=\frac{2E_{\mathrm{A}}}{E_{\mathrm{A}}+E_{\mathrm{C}}}=1-\frac{\tau_2}{\tau_1} \quad \text{(using equations (4) and (5)).} \tag{31}$$

Case (iii): $A=0$. This case has a high-wave-number component present in each region as well as the low-wave-number wave in region 2. The wave amplitudes B and C will be given in terms of D since only this wave transports energy towards the interface. The solutions will be given in terms of γ_A (or E_A) and γ_C (or E_C) even though the wave A is not present, as well as in terms of γ_B (or E_B) and γ_C (or E_C). The solution of equations (21) and (25) gives

$$\frac{C}{D}=\frac{E_C-E_A}{E_C+E_A}=\frac{E_C+E_B}{E_C-E_B}=\frac{\tau_2}{\tau_1} \quad \text{(using equations (4) and (5)),} \tag{32}$$

$$\frac{B}{D}=\frac{2E_C}{E_A+E_C}=\frac{2E_C}{E_C-E_B}=\frac{1}{\tau_1} \quad \text{(using equation (5)).} \tag{33}$$

(Alternatively from equations (4) and (5), $D/B=\tau_1$ and $C/B=\tau_2$.)

This case was partly verified by experiment in Part I with just one test using a mesh expansion (Figure 11) and another test using a mesh contraction (Figure 14). Four more tests are contained in the present paper.

Case (iv): $C=0$. This case also has a high-wave-number component present in each region. In addition there is a low-wave-number component in region 1. The amplitudes of the high-wave-number waves B and D will be determined as a function of the incident amplitude A. The solution of equations (21) and (25) gives

$$\frac{B}{A}=\frac{E_A+E_C}{E_A-E_C}=\frac{E_A-E_D}{E_A+E_D}=\frac{-\tau_1}{\tau_2} \quad \text{(using equation (5)),} \tag{34}$$

$$\frac{D}{A}=\frac{2E_A}{E_A-E_C}=\frac{2E_A}{E_A+E_D}=1-\frac{\tau_1}{\tau_2} \quad \text{(using equations (4) and (5)).} \tag{35}$$

3.5. *Discussion of the four solutions*

It has been demonstrated in the analysis that based upon *group velocity* (or long and short waves) there are four possible solutions or wave configurations, each containing three waves. From the viewpoint of *phase velocity* (in which there are only two discernible wave configurations) all the waves present in all four cases are travelling in the same $+x$-direction (see Figure 6). In cases (i) and (iii) an incident wave in region 1 gives rise to two transmitted waves in region 2. In cases (ii) and (iv) there are two incident waves in region 1 but only one transmitted wave in region 2. From the viewpoint of *energy velocity*, however, each case has waves in which the energy flux is in both directions. Those energy velocities in the $-x$-direction are associated with the high-wave-number components, i.e. waves B and D.

In the 'hot-start' solution or case (i), the incident wave A transports energy towards the interface in region 1. In region 2 the long-wavelength wave C carries energy away from the interface, but at the same time the short-wavelength wave D transports energy towards the interface. It is clear that in order to sustain this configuration of waves indefinitely, *two* energy sources would be required—one at the upstream end of region 1 and the other at the downstream end of region 2.

In the 'cold-start' solution or case (ii), the long-wavelength incident wave A carries energy towards the interface. At the interface this energy is redistributed between the high-wave-number wave B in region 1 and the low-wave-number wave C in region 2. Thus it is seen that only *one* energy source is required and this is at the upstream end of region 1.

Case (iii) contains a high-wave-number component (i.e. wave B) in region 1, which transports energy upstream away from the interface. In region 2 the energy flux due to the waves with amplitudes C and D is away from and towards the interface respectively. This case is similar to case (ii) in that only a *single* energy source is required, this time at the downstream end of region 2. Although no experiments have been carried out, it seems likely that if the velocities and surface elevations were set to zero in region 1 (i.e. a 'cold-start') and if a short-wavelength wave with dimensionless wave number γ_D were present in region 2, a numerical model would probably generate wave B in region 1 and wave C in region 2 if the model was run for a sufficiently long time. This case provides an interesting example of a high-wave-number component giving rise to a low-wave-number component—a process which is also a characteristic of negative diffusion!

Case (iv) contains waves A and B in region 1 and only wave D in region 2. Like case (i), this particular configuration of waves requires *two* energy sources. Energy is transported towards the interface by waves A and D and away from the interface by wave B.

It is an interesting point as to why the analysis of Part I singled out cases (i) and (iii) as valid solutions in preference to cases (ii) and (iv). The reason lies in the form of the assumed solution, which only allowed for one incident wave rather than two waves (incident, that is, in terms of phase rather than energy flux). Thus cases (ii) and (iv) were automatically excluded.

4. NUMERICAL EXPERIMENTS FOR THE GENERALIZED ANALYSIS

Numerical experiments for case (i) with $B=0$ were described in Part I. Experiments to test the validity of cases (ii), (iii) and (iv) were needed. Additionally, for case (ii) where $D=0$, the solutions from the numerical model with the initial conditions determined by the analysis (equations (14)–(19), (30) and (31)) will be compared with those obtained with 'cold-start' initial conditions in which only wave A was present. In region 2 the initial velocities and surface elevations were set to zero. The model was then run for a period of time until the transients were less significant.

The analyses for cases (iii) with $A=0$ and (iv) with $C=0$ were also tested with some ('hot-start') numerical experiments. For case (iii) the initial conditions were defined by equations (14)–(19), (32) and (33). For case (iv) the initial conditions were specified by equations (14)–(19), (34) and (35).

4.1. Data used in the numerical experiments

The data for the different wave configurations of cases (ii), (iii) and (iv) are given in Tables II, III and IV respectively. In all three tables, $H'=\Delta x_2/\Delta x_1$ is the mesh size ratio and N_x is the dimensionless wavelength.

4.2. Results and conclusions of the numerical experiments for the generalized analysis

The results of the ('hot-start') numerical experiments for cases (ii), (iii) and (iv) are contained in Figures 1(b)–4(b), 7–10 and 11–14 respectively. The difference between the values from the finite element model and the values predicted from the analysis have been plotted as a small triangle at each node. In all cases and for all times displayed, the results showed that there was no difference between the two sets of values. This verifies the validity of the solutions of all four cases contained in equations (28)–(35).

The results for case (ii) will now be considered further. Figures 1(a)–4(a) contain the results of the ('cold-start') numerical experiments in which the initial conditions consisted of only one wave and this was the incident wave in region 1. In region 2 the surface elevations and velocities were initially set to zero. The tests were run for a sufficiently long time for a pseudo-steady state condition to be reached just downstream of the interface. Figures 1(b)–4(b) display the results of the corresponding ('hot-start') numerical experiments discussed in Section 2 in which the initial

Table II. Case (ii): $D=0$

	Mesh expansion, $H'=2$	Mesh contraction, $H'=1/2$
$N_x=4$	$L_c/\Delta x_2=4{\cdot}0000$ $L_A/\Delta x_1=8{\cdot}3617$ $L_B/\Delta x_1=2{\cdot}1816$ $A=1{\cdot}0000$ $B=0{\cdot}2864$ $C=1{\cdot}2864$ (Figure 1(b))	$L_A/\Delta x_1=4{\cdot}0000$ $L_B/\Delta x_1=2{\cdot}5152$ $L_c/\Delta x_2=8{\cdot}3617$ $A=1{\cdot}0000$ $B=-0{\cdot}2864$ $C=0{\cdot}7136$ (Figure 3(b))
$N_x=8$	$L_c/\Delta x_2=8{\cdot}0000$ $L_A/\Delta x_1=16{\cdot}0343$ $L_B/\Delta x_1=2{\cdot}0878$ $A=1{\cdot}0000$ $B=0{\cdot}0441$ $C=1{\cdot}0441$ (Figure 2(b))	$L_A/\Delta x_1=8{\cdot}0000$ $L_B/\Delta x_2=2{\cdot}1914$ $L_c/\Delta x_2=16{\cdot}0343$ $A=1{\cdot}0000$ $B=-0{\cdot}0441$ $C=0{\cdot}9559$ (Figure 4(b))

Table III. Case (iii): $A=0$

	Mesh expansion, $H'=2$	Mesh contraction, $H'=1/2$
$N_x=4$	$L_c/\Delta x_2=4{\cdot}0000$ $L_A/\Delta x_1=8{\cdot}3617$ $L_B/\Delta x_1=2{\cdot}1816$ $L_D/\Delta x_2=2{\cdot}5152$ $B=0{\cdot}7136$ $C=-0{\cdot}2864$ $D=1{\cdot}0000$ (Figure 7)	$L_A/\Delta x_1=4{\cdot}0000$ $L_B/\Delta x_1=2{\cdot}1914$ $L_c/\Delta x_2=16{\cdot}0343$ $L_D/\Delta x_2=2{\cdot}0878$ $B=1{\cdot}2864$ $C=0{\cdot}2864$ $D=1{\cdot}0000$ (Figure 9)
$N_x=8$	$L_c/\Delta x_2=8{\cdot}0000$ $L_A/\Delta x_1=16{\cdot}0343$ $L_B/\Delta x_1=2{\cdot}0878$ $L_D/\Delta x_2=2{\cdot}1914$ $B=0{\cdot}9559$ $C=-0{\cdot}0441$ $D=1{\cdot}0000$ (Figure 8)	$L_A/\Delta x_1=8{\cdot}0000$ $L_B/\Delta x_1=2{\cdot}1914$ $L_c/\Delta x_2=16{\cdot}0343$ $L_D/\Delta x_2=2{\cdot}0878$ $B=1{\cdot}0441$ $C=0{\cdot}0441$ $D=1{\cdot}0000$ (Figure 10)

conditions were defined by equations (14)–(19), (30) and (31). When these figures are compared qualitatively with the corresponding true cold-start experiments (Figures 1(a)–4(a)), it is evident that the analysis for case (ii) provides a true description of the waves which are being established as time progresses in the 'cold-start' experiments.

The results of the numerical experiments for cases (iii) and (iv) are contained in Figures 7–10 and 11–14 respectively. Case (iii) is interesting in that, like case (ii), it requires only one source of energy. Wave D is the provider of this energy, which is then redistributed between waves B and C at the interface. It is only case (iii) which satisfies the requirements that the sole energy source is located in region 2 and energy is pumped from region 2 to region 1. In a similar manner, it is only case (ii)

Table IV. Case (iv): $C=0$

	Mesh expansion, $H'=2$	Mesh contraction, $H'=1/2$
$N_x=4$	$L_c/\Delta x_2=4{\cdot}0000$ $L_A/\Delta x_1=8{\cdot}3617$ $L_B/\Delta x_1=2{\cdot}1816$ $L_D/\Delta x_2=2{\cdot}5152$ $A=1{\cdot}0000$ $B=3{\cdot}4914$ $D=4{\cdot}4914$ (Figure 11)	$L_A/\Delta x_1=4{\cdot}0000$ $L_B/\Delta x_1=2{\cdot}5152$ $L_c/\Delta x_2=8{\cdot}3617$ $L_D/\Delta x_2=2{\cdot}1816$ $A=1{\cdot}0000$ $B=-3{\cdot}4914$ $D=-2{\cdot}4914$ (Figure 13)
$N_x=8$	$L_c/\Delta x_2=8{\cdot}0000$ $L_A/\Delta x_1=16{\cdot}0343$ $L_B/\Delta x_1=2{\cdot}0878$ $L_D/\Delta x_2=2{\cdot}1914$ $A=1{\cdot}0000$ $B=22{\cdot}6790$ $D=23{\cdot}6790$ (Figure 12)	$L_A/\Delta x_1=8{\cdot}0000$ $L_B/\Delta x_1=2{\cdot}1914$ $L_c/\Delta x_2=16{\cdot}0343$ $L_D/\Delta x_2=2{\cdot}0878$ $A=1{\cdot}0000$ $B=-22{\cdot}6790$ $D=-21{\cdot}6790$ (Figure 14)

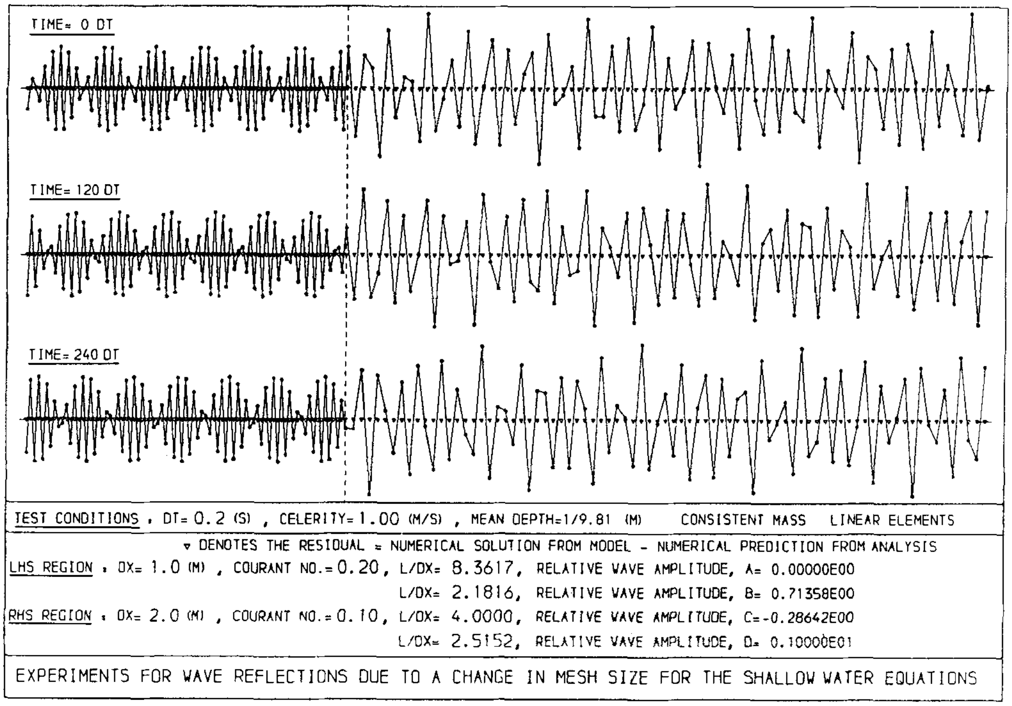

```
TEST CONDITIONS , DT= 0.2 (S) , CELERITY= 1.00 (M/S) , MEAN DEPTH=1/9.81 (M)    CONSISTENT MASS   LINEAR ELEMENTS
                 ▿ DENOTES THE RESIDUAL = NUMERICAL SOLUTION FROM MODEL - NUMERICAL PREDICTION FROM ANALYSIS
LHS REGION , DX= 1.0 (M) , COURANT NO.=0.20, L/DX= 8.3617, RELATIVE WAVE AMPLITUDE, A= 0.00000E00
                                             L/DX= 2.1816, RELATIVE WAVE AMPLITUDE, B= 0.71358E00
RHS REGION , DX= 2.0 (M) , COURANT NO.=0.10, L/DX= 4.0000, RELATIVE WAVE AMPLITUDE, C=-0.28642E00
                                             L/DX= 2.5152, RELATIVE WAVE AMPLITUDE, D= 0.10000E01
EXPERIMENTS FOR WAVE REFLECTIONS DUE TO A CHANGE IN MESH SIZE FOR THE SHALLOW WATER EQUATIONS
```

Figure 7. Mesh refinement test with hot start for case (iii) with $A=0$. Waves present are: incident wave B ($2{\cdot}1816\Delta x_1$) and transmitted waves C ($4{\cdot}0000\Delta x_2$) and D ($2{\cdot}5152\Delta x_2$)

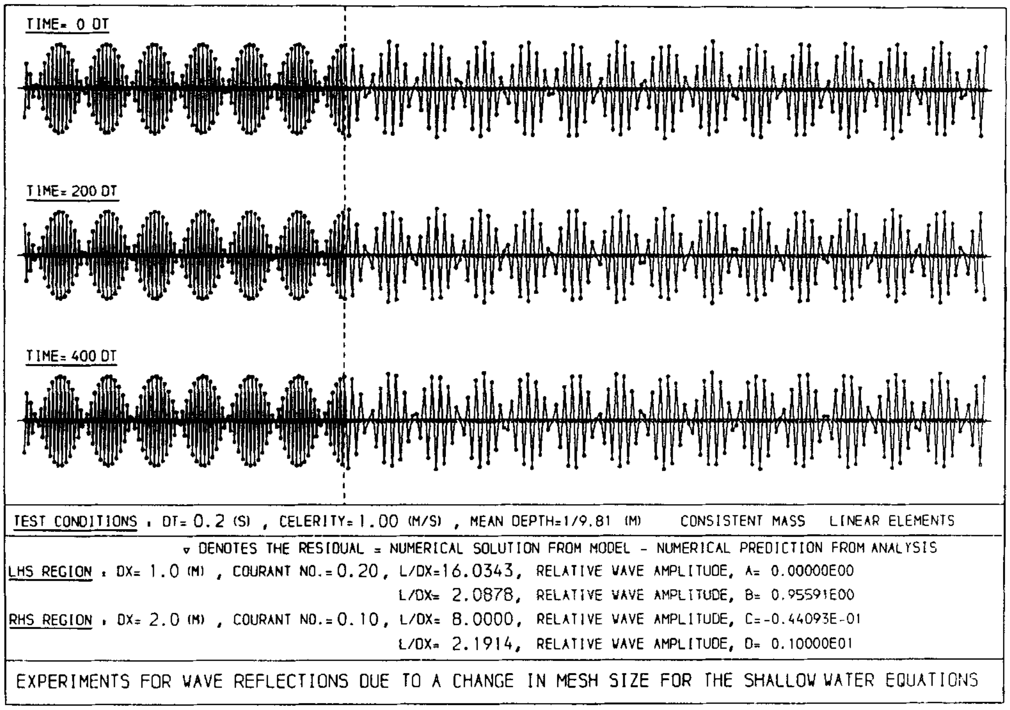

TEST CONDITIONS , DT= 0.2 (S) , CELERITY= 1.00 (M/S) , MEAN DEPTH=1/9.81 (M) CONSISTENT MASS LINEAR ELEMENTS

∇ DENOTES THE RESIDUAL = NUMERICAL SOLUTION FROM MODEL - NUMERICAL PREDICTION FROM ANALYSIS

LHS REGION , DX= 1.0 (M) , COURANT NO.=0.20, L/DX=16.0343, RELATIVE WAVE AMPLITUDE, A= 0.00000E00
L/DX= 2.0878, RELATIVE WAVE AMPLITUDE, B= 0.95591E00
RHS REGION , DX= 2.0 (M) , COURANT NO.=0.10, L/DX= 8.0000, RELATIVE WAVE AMPLITUDE, C=-0.44093E-01
L/DX= 2.1914, RELATIVE WAVE AMPLITUDE, D= 0.10000E01

EXPERIMENTS FOR WAVE REFLECTIONS DUE TO A CHANGE IN MESH SIZE FOR THE SHALLOW WATER EQUATIONS

Figure 8. Mesh refinement test with hot start for case (iii) with $A = 0$. Waves present are: incident wave B ($2{\cdot}0878\Delta x_1$) and transmitted waves C ($8{\cdot}0000\Delta x_2$) and D ($2{\cdot}1914\Delta x_2$)

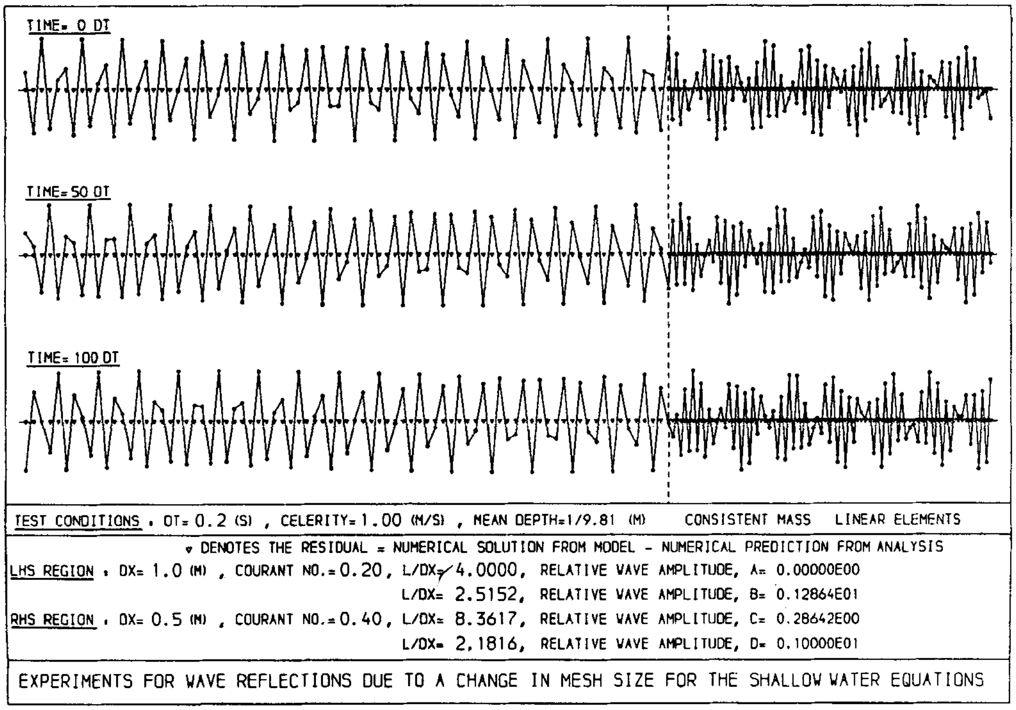

TEST CONDITIONS , DT= 0.2 (S) , CELERITY= 1.00 (M/S) , MEAN DEPTH=1/9.81 (M) CONSISTENT MASS LINEAR ELEMENTS

∇ DENOTES THE RESIDUAL = NUMERICAL SOLUTION FROM MODEL - NUMERICAL PREDICTION FROM ANALYSIS

LHS REGION , DX= 1.0 (M) , COURANT NO.=0.20, L/DX=4.0000, RELATIVE WAVE AMPLITUDE, A= 0.00000E00
L/DX= 2.5152, RELATIVE WAVE AMPLITUDE, B= 0.12864E01
RHS REGION , DX= 0.5 (M) , COURANT NO.=0.40, L/DX= 8.3617, RELATIVE WAVE AMPLITUDE, C= 0.28642E00
L/DX= 2.1816, RELATIVE WAVE AMPLITUDE, D= 0.10000E01

EXPERIMENTS FOR WAVE REFLECTIONS DUE TO A CHANGE IN MESH SIZE FOR THE SHALLOW WATER EQUATIONS

Figure 9. Mesh refinement test with hot start for case (iii) with $A = 0$. Waves present are: incident wave B ($2{\cdot}5152\Delta x_1$) and transmitted waves C ($8{\cdot}3617\Delta x_2$) and D ($2{\cdot}1816\Delta x_2$)

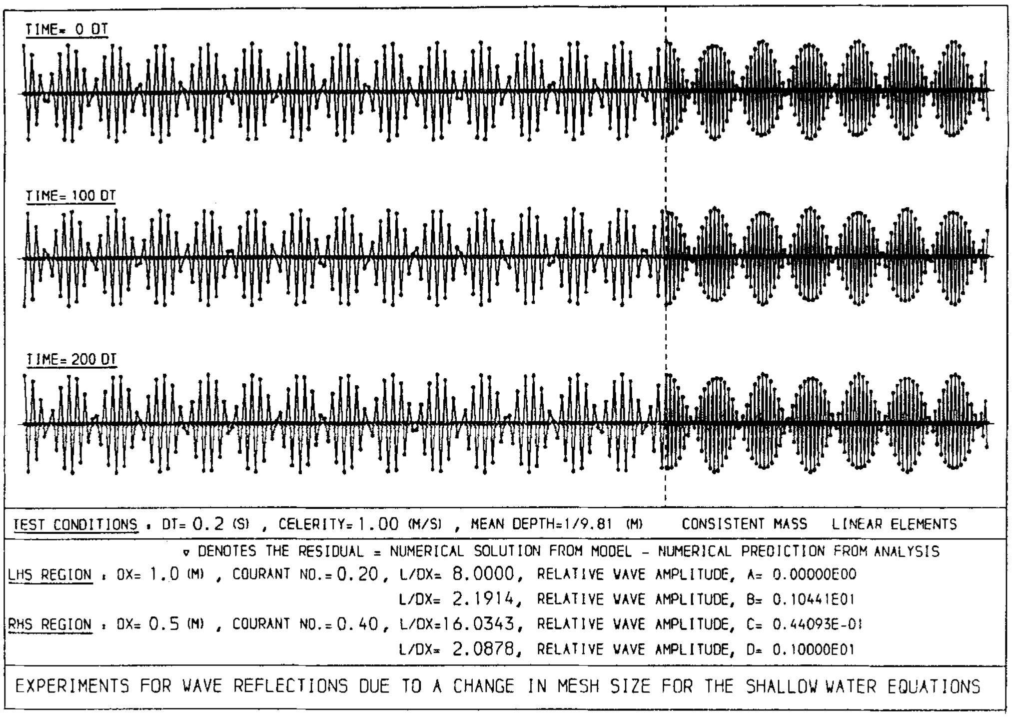

```
TEST CONDITIONS , DT= 0.2 (S) , CELERITY= 1.00 (M/S) , MEAN DEPTH=1/9.81 (M)     CONSISTENT MASS    LINEAR ELEMENTS
                    ▿ DENOTES THE RESIDUAL = NUMERICAL SOLUTION FROM MODEL - NUMERICAL PREDICTION FROM ANALYSIS
LHS REGION : DX= 1.0 (M) , COURANT NO.= 0.20, L/DX= 8.0000, RELATIVE WAVE AMPLITUDE, A= 0.00000E00
                                              L/DX= 2.1914, RELATIVE WAVE AMPLITUDE, B= 0.10441E01
RHS REGION : DX= 0.5 (M) , COURANT NO.= 0.40, L/DX=16.0343, RELATIVE WAVE AMPLITUDE, C= 0.44093E-01
                                              L/DX= 2.0878, RELATIVE WAVE AMPLITUDE, D= 0.10000E01
EXPERIMENTS FOR WAVE REFLECTIONS DUE TO A CHANGE IN MESH SIZE FOR THE SHALLOW WATER EQUATIONS
```

Figure 10. Mesh refinement test with hot start for case (iii) with $A = 0$. Waves present are: incident wave B ($2{\cdot}1914\Delta x_1$) and transmitted waves C ($16{\cdot}0343\Delta x_2$) and D ($2{\cdot}0878\Delta x_2$)

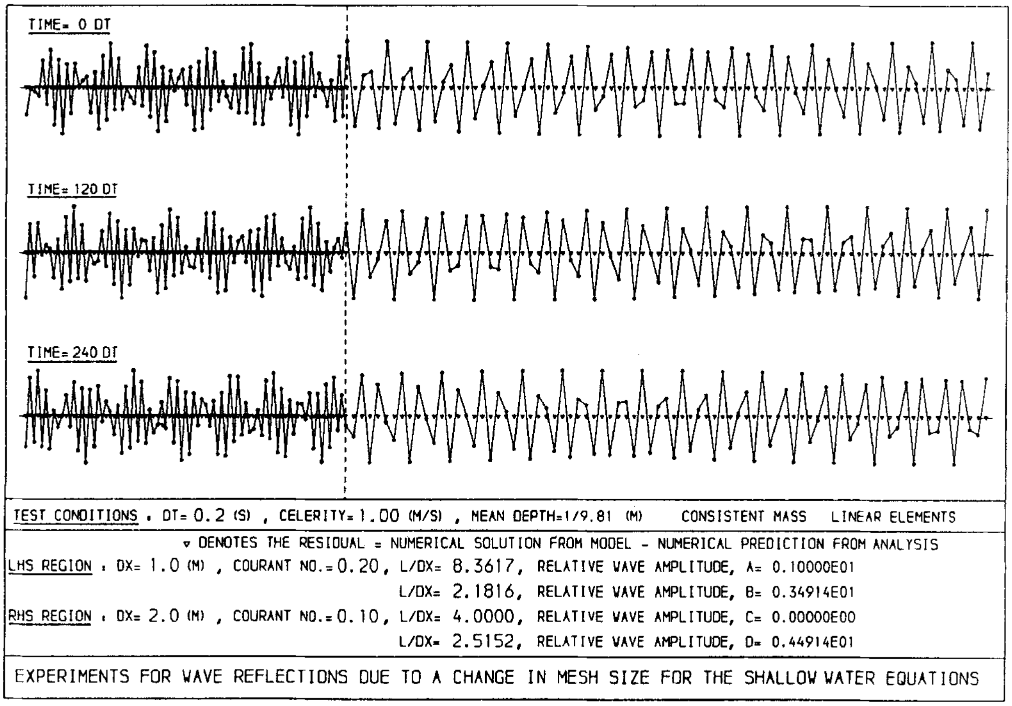

```
TEST CONDITIONS , DT= 0.2 (S) , CELERITY= 1.00 (M/S) , MEAN DEPTH=1/9.81 (M)     CONSISTENT MASS    LINEAR ELEMENTS
                    ▿ DENOTES THE RESIDUAL = NUMERICAL SOLUTION FROM MODEL - NUMERICAL PREDICTION FROM ANALYSIS
LHS REGION : DX= 1.0 (M) , COURANT NO.= 0.20, L/DX= 8.3617, RELATIVE WAVE AMPLITUDE, A= 0.10000E01
                                              L/DX= 2.1816, RELATIVE WAVE AMPLITUDE, B= 0.34914E01
RHS REGION : DX= 2.0 (M) , COURANT NO.= 0.10, L/DX= 4.0000, RELATIVE WAVE AMPLITUDE, C= 0.00000E00
                                              L/DX= 2.5152, RELATIVE WAVE AMPLITUDE, D= 0.44914E01
EXPERIMENTS FOR WAVE REFLECTIONS DUE TO A CHANGE IN MESH SIZE FOR THE SHALLOW WATER EQUATIONS
```

Figure 11. Mesh refinement test with hot start for case (iv) with $C = 0$. Waves present are: incident waves A ($8{\cdot}3617\Delta x_1$) and B ($2{\cdot}1816\Delta x_1$) and transmitted wave D ($2{\cdot}5152\Delta x_2$)

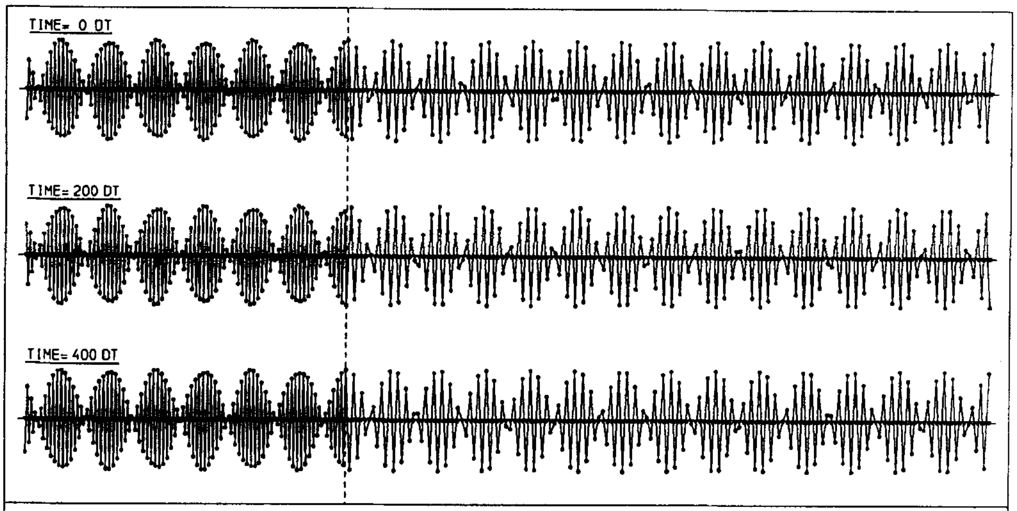

TEST CONDITIONS , DT= 0.2 (S) , CELERITY= 1.00 (M/S) , MEAN DEPTH=1/9.81 (M) CONSISTENT MASS LINEAR ELEMENTS

▿ DENOTES THE RESIDUAL = NUMERICAL SOLUTION FROM MODEL - NUMERICAL PREDICTION FROM ANALYSIS

LHS REGION , DX= 1.0 (M) , COURANT NO.= 0.20, L/DX=16.0343, RELATIVE WAVE AMPLITUDE, A= 0.10000E01
L/DX= 2.0878, RELATIVE WAVE AMPLITUDE, B= 0.22679E02
RHS REGION , DX= 2.0 (M) , COURANT NO.= 0.10, L/DX= 8.0000, RELATIVE WAVE AMPLITUDE, C= 0.00000E00
L/DX= 2.1914, RELATIVE WAVE AMPLITUDE, D= 0.23679E02

EXPERIMENTS FOR WAVE REFLECTIONS DUE TO A CHANGE IN MESH SIZE FOR THE SHALLOW WATER EQUATIONS

Figure 12. Mesh refinement test with hot start for case (iv) with $C=0$. Waves present are: incident waves A ($16{\cdot}0343\Delta x_1$) and B ($2{\cdot}0878\Delta x_1$) and transmitted wave D ($2{\cdot}1914\Delta x_2$)

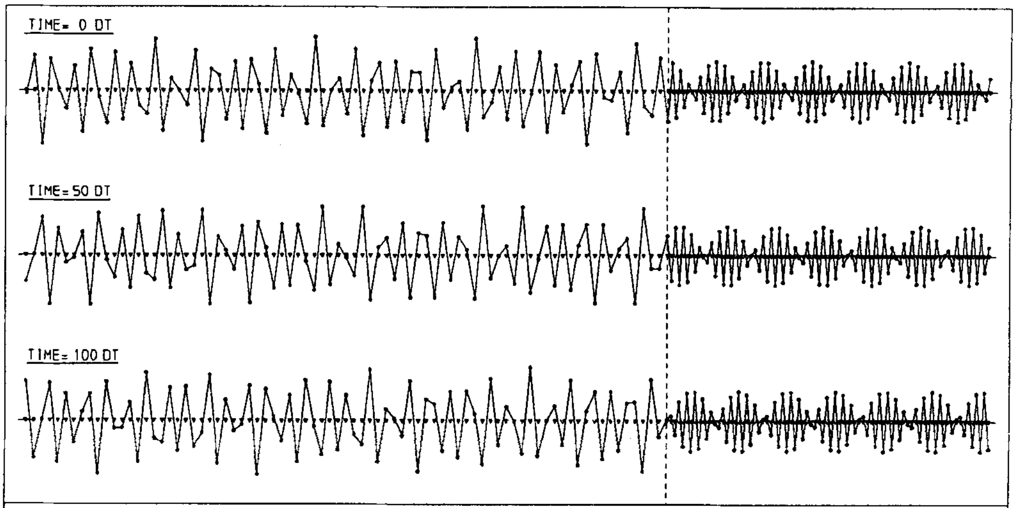

TEST CONDITIONS , DT= 0.2 (S) , CELERITY= 1.00 (M/S) , MEAN DEPTH=1/9.81 (M) CONSISTENT MASS LINEAR ELEMENTS

▿ DENOTES THE RESIDUAL = NUMERICAL SOLUTION FROM MODEL - NUMERICAL PREDICTION FROM ANALYSIS

LHS REGION , DX= 1.0 (M) , COURANT NO.= 0.20, L/DX= 4.0000, RELATIVE WAVE AMPLITUDE, A= 0.10000E01
L/DX= 2.5152, RELATIVE WAVE AMPLITUDE, B=-0.34914E01
RHS REGION , DX= 0.5 (M) , COURANT NO.= 0.40, L/DX= 8.3617, RELATIVE WAVE AMPLITUDE, C= 0.00000E00
L/DX= 2.1816, RELATIVE WAVE AMPLITUDE, D=-0.24914E01

EXPERIMENTS FOR WAVE REFLECTIONS DUE TO A CHANGE IN MESH SIZE FOR THE SHALLOW WATER EQUATIONS

Figure 13. Mesh refinement test with hot start for case (iv) with $C=0$. Waves present are: incident waves A ($4{\cdot}0000\Delta x_1$) and B ($2{\cdot}5152\Delta x_1$) and transmitted wave D ($2{\cdot}1816\Delta x_2$)

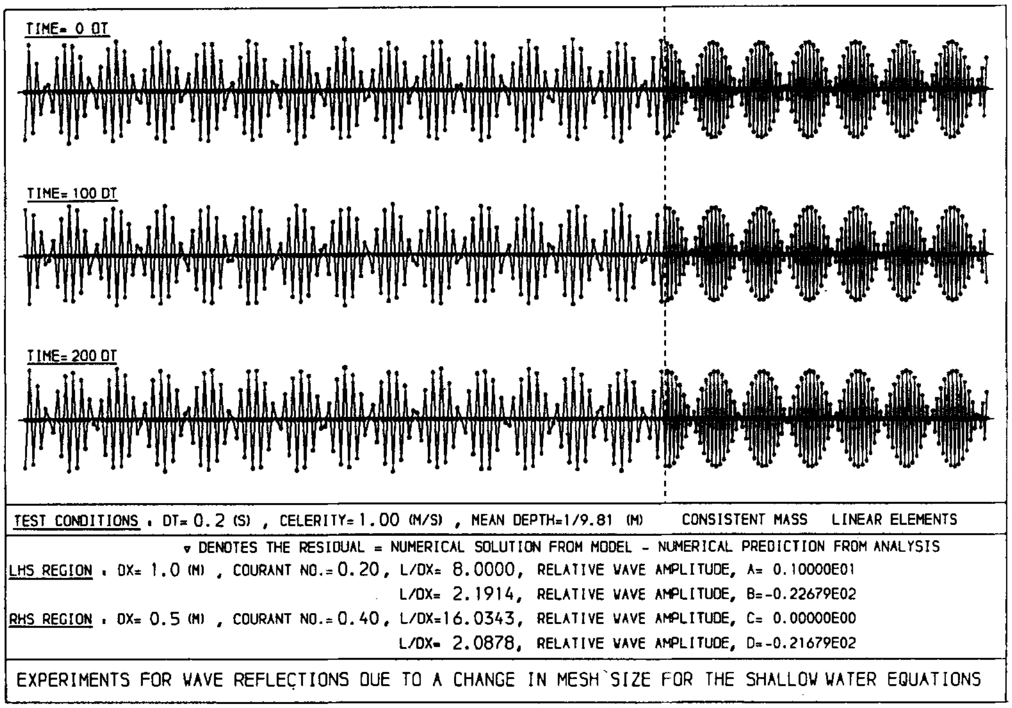

TEST CONDITIONS . DT= 0.2 (S) , CELERITY= 1.00 (M/S) , MEAN DEPTH=1/9.81 (M) CONSISTENT MASS LINEAR ELEMENTS

▿ DENOTES THE RESIDUAL = NUMERICAL SOLUTION FROM MODEL - NUMERICAL PREDICTION FROM ANALYSIS

LHS REGION . DX= 1.0 (M) , COURANT NO.= 0.20, L/DX= 8.0000, RELATIVE WAVE AMPLITUDE, A= 0.10000E01
L/DX= 2.1914, RELATIVE WAVE AMPLITUDE, B=-0.22679E02
RHS REGION . DX= 0.5 (M) , COURANT NO.= 0.40, L/DX=16.0343, RELATIVE WAVE AMPLITUDE, C= 0.00000E00
L/DX= 2.0878, RELATIVE WAVE AMPLITUDE, D=-0.21679E02

EXPERIMENTS FOR WAVE REFLECTIONS DUE TO A CHANGE IN MESH`SIZE FOR THE SHALLOW WATER EQUATIONS

Figure 14. Mesh refinement test with hot start for case (iv) with $C=0$. Waves present are: incident waves A ($8{\cdot}0000\Delta x_1$) and B ($2{\cdot}1914\Delta x_1$) and transmitted wave D ($2{\cdot}0878\Delta x_2$)

which could be activated by a 'cold-start' in which the only energy source is in region 1 and energy is being fed towards the interface from region 1.

Case (iv) contained the largest waves which were generated. Of the waves present, the magnitudes varied from unity to 23·7 and it is rather surprising that such examples could be valid. Since the system is linear, it is possible that the amplitude of some of the waves generated exceeded the fluid depth! Cases (iv) and (i) would require *both* upstream and downstream energy sources. In the context of a simulation of a real estuary using a varying grid size, it is likely that all four cases would be present to an extent which would depend upon the waves present and hence the effective energy sources present.

5. CONCLUSIONS

The generalized reflection analysis provides a better understanding of the processes at work when there is a change in mesh size in a one-dimensional Crank–Nicolson linear finite element model. The conclusions are:

1. The method of analysis would be applicable to other numerical schemes which possess a dispersion relation which is concave down. Such dispersion relations have two wave numbers corresponding to each wave frequency. (The analysis for numerical schemes with a monotonic increasing dispersion relation is simpler since there is only one wave number for each wave frequency.)

2. The wave numbers in the two regions can be related to each other via the dispersion relation. It has been shown that for Crank–Nicolson linear finite elements in the situation of a mesh expansion, there is a band of real wave numbers for the incident wave which give rise to complex wave numbers in the downstream region. Such 'evanescent' waves are damped in space and arise because the frequency of oscillation of the interfacial node is too high for the numerical scheme to resolve in the downstream region. (Evanescent waves are discussed in Part III.)
3. Expressions for the transmission coefficients have been derived (equations (6) and (7)). These show that the transmission coefficients depend only upon the wave numbers in both regions and the mesh size ratio (which also equals the ratio of the Courant numbers in both regions). Thus the transmission coefficients depend on the relative and not the absolute values of the Courant numbers. Equations (28)–(35) permit the effects on wave amplitude to be quantified due to any change in mesh size for any wavelength and wave configuration. Equations (16)–(20) in Part I can be used to quantify the effects of a mesh size change on the wavelengths in both regions.

   For example, consider the effects of a *mesh expansion* with a mesh size ratio of 2 on incident waves with wavelengths $2{\cdot}1\Delta x_1$, $4\Delta x_1$ and $8\Delta x_1$. The resulting wave amplitudes are given in Table V for cases (i) and (ii).

   For a *mesh contraction* with a mesh size ratio of 0·5, the corresponding amplitudes resulting from incident waves with wavelengths $2{\cdot}1\Delta x_1$, $4\Delta x_1$ and $8\Delta x_1$ are given in Table VI for cases (i) and (ii).

   A comparison within each of Tables V and VI as well as between tables reveals the extraordinary variety in the behaviour of the resultant wave patterns caused by the change in mesh size.

Table V. Mesh expansion

	Wavelength of incident wave A		
	$2{\cdot}1\Delta x_1$	$4\Delta x_1$	$8\Delta x_1$
Case (i) $B=0$	$C/A=\tau_1=-0{\cdot}0622$ $D/A=\tau_2=1{\cdot}0622$	Wave numbers in region 2 are complex, indicating a damped-in-space wave (to be considered in Part III)	$C/A=\tau_1=1{\cdot}5473$ $D/A=\tau_2=-0{\cdot}5473$
Case (ii) ('cold-start') $D=0$	$B/A=-\tau_2/\tau_1=17{\cdot}0653$ $C/A=1-\tau_2/\tau_1=18{\cdot}0653$		$B/A=-\tau_2/\tau_1=0{\cdot}3537$ $C/A=1-\tau_2/\tau_1=1{\cdot}3537$

Table VI. Mesh contraction

	Wavelength of incident wave A		
	$2{\cdot}1\Delta x_1$	$4\Delta x_1$	$8\Delta x_1$
Case (i) $B=0$	$C/A=\tau_1=0{\cdot}0071$ $D/A=\tau_2=0{\cdot}9929$	$C/A=\tau_1=0{\cdot}7774$ $D/A=\tau_2=0{\cdot}2226$	$C/A=\tau_1=0{\cdot}9578$ $D/A=\tau_2=0{\cdot}0422$
Case (ii) ('cold-start') $D=0$	$B/A=-\tau_2/\tau_1=-139{\cdot}11$ $C/A=1-\tau_2/\tau_1=-138{\cdot}11$	$B/A=-\tau_2/\tau_1=-0{\cdot}2864$ $C/A=1-\tau_2/\tau_1=0{\cdot}7136$	$B/A=-\tau_2/\tau_1=-0{\cdot}0441$ $C/A=1-\tau_2/\tau_1=0{\cdot}9559$

4. The energy velocity (or group velocity) is a more fundamental quantity than phase velocity as far as wave reflections and transmissions are concerned. On an *energy flux* basis, four distinct wave configurations were identified, i.e. cases (i)–(iv)—see Figure 6. Cases (ii) and (iii) required one energy source and would therefore be activated by a cold-start in a numerical model. Cases (i) and (iv) required both an upstream and downstream energy source. They would only be activated once a numerical model had been running for some time when, due to reflections from model boundaries, etc., the requirements for two energy sources derived from waves travelling in the same direction in the 1D model would be satisfied.
5. Based upon *phase velocity*, there are just two discernible wave configurations, viz. case (i) or (iii) and case (ii) or (iv). Since there are no internally reflected waves in any of the wave configurations, all waves travel in the downstream direction.
6. As shown in Part I, the energy flux is balanced across the interfacial node for case (i) and consequently, by superposition, for the other three cases as well.

REFERENCES

1. B. Cathers, S. Bates and B. A. O'Connor, 'Internal wave reflections and transmissions arising from a non-uniform mesh. Part I: An analysis for the Crank–Nicolson linear finite element scheme', *Int. j. numer. methods fluids*, **9**, 783–810 (1989).